

## KELT-7b: A HOT JUPITER TRANSITING A BRIGHT V=8.54 RAPIDLY ROTATING F-STAR

ALLYSON BIERYLA<sup>1</sup>, KAREN COLLINS<sup>2</sup>, THOMAS G. BEATTY<sup>3</sup>, JASON EASTMAN<sup>1,4</sup>, ROBERT J. SIVERD<sup>4</sup>, JOSHUA PEPPER<sup>6</sup>,  
B. SCOTT GAUDI<sup>7</sup>, KEIVAN G. STASSUN<sup>5,8</sup>, CALEB CAÑAS<sup>1</sup>, DAVID W. LATHAM<sup>1</sup>, LARS A. BUCHHAVE<sup>1,9</sup>, ROBERTO  
SANCHIS-OJEDA<sup>10,11</sup>, JOSHUA N. WINN<sup>12</sup>, ERIC L. N. JENSEN<sup>13</sup>, JOHN F. KIELKOPF<sup>2</sup>, KIM K. MCLEOD<sup>14</sup>, JOAO GREGORIO<sup>15</sup>,  
KNICOLE D. COLÓN<sup>6</sup>, RACHEL STREET<sup>4</sup>, RACHEL ROSS<sup>4</sup>, MATTHEW PENNY<sup>7</sup>, SAMUEL N. MELLON<sup>16</sup>, THOMAS E. OBERST<sup>16</sup>,  
BENJAMIN J. FULTON<sup>17,18</sup>, JI WANG<sup>19</sup>, PERRY BERLIND<sup>1</sup>, MICHAEL L. CALKINS<sup>1</sup>, GILBERT A. ESQUERDO<sup>1</sup>, DARREN L.  
DEPOY<sup>20</sup>, ANDREW GOULD<sup>7</sup>, JENNIFER MARSHALL<sup>20</sup>, RICHARD POGGE<sup>7</sup>, MARK TRUEBLOOD<sup>21</sup>, PATRICIA TRUEBLOOD<sup>21</sup>

*Draft version February 25, 2020*

### ABSTRACT

We report the discovery of KELT-7b, a transiting hot Jupiter with a mass of  $1.28 \pm 0.18 M_J$ , radius of  $1.533^{+0.046}_{-0.047} R_J$ , and an orbital period of  $2.7347749 \pm 0.0000039$  days. The bright host star (HD 33643; KELT-7) is an F-star with  $V = 8.54$ ,  $T_{\text{eff}} = 6789^{+50}_{-49}$  K,  $[\text{Fe}/\text{H}] = 0.139^{+0.075}_{-0.081}$ , and  $\log g = 4.149 \pm 0.019$ . It has a mass of  $1.535^{+0.066}_{-0.054} M_{\odot}$ , a radius of  $1.732^{+0.043}_{-0.045} R_{\odot}$ , and is the fifth most massive, fifth hottest, and the ninth brightest star known to host a transiting planet. It is also the brightest star around which KELT has discovered a transiting planet. Thus, KELT-7b is an ideal target for detailed characterization given its relatively low surface gravity, high equilibrium temperature, and bright host star. The rapid rotation of the star ( $73 \pm 0.5 \text{ km s}^{-1}$ ) results in a Rossiter-McLaughlin effect with an unusually large amplitude of several hundred  $\text{m s}^{-1}$ . We find that the orbit normal of the planet is likely to be well-aligned with the stellar spin axis, with a projected spin-orbit alignment of  $\lambda = 9.7 \pm 5.2$  degrees. This is currently the most rapidly rotating star to have a reflex signal (and thus mass determination) due to a planetary companion measured.

*Subject headings:* planetary systems — stars: individual (KELT) techniques: spectroscopic, photometric

### 1. INTRODUCTION

Transiting planets that orbit bright host stars are of great value to the exoplanet community. Bright host stars are ideal candidates for follow-up because the higher photon flux generally allows for a wider array of follow-up observations, more precise determination of physical parameters, and better ability to diagnose and control systematic errors. As a result, bright transiting systems have proven to be important laboratories for studying atmospheric properties of the planet through transmission and emission spectroscopy, for measuring the spin-orbit alignment of the planet orbits, and for determining precise stellar parameters (see Winn 2011 for review).

The Kilodegree Extremely Little Telescope (KELT) transit survey (Pepper et al. 2007) was designed to detect transiting planets around bright ( $8 < V < 10$ ) stars. Very few ( $\sim 3\%$ ) of the known transiting-hosting stars are in this brightness range. This is because this range spans the gap between radial velocity surveys on the bright end, and the saturation limit of the majority of ground-based transit surveys on the faint end. The KELT-North (KELT-N) telescope targets this range using a small-aperture (42 mm) camera with a wide field of view of  $26^{\circ} \times 26^{\circ}$ . It observes 13 fields at declination of 31.7 degrees, roughly equally spaced in right ascension, in total covering approximately 40% of the Northern sky. The KELT-N survey has been in operation since 2006 and candidates have been actively vetted since April 2011.

The KELT-N survey has already announced four planet discoveries. KELT-1b (Siverd et al. 2012) is a  $27 M_J$  brown dwarf transiting a  $V = 10.7$  F-star. KELT-2Ab (Beatty et al. 2012) is a hot Jupiter transiting the bright ( $V = 8.77$ ) primary star in a visual binary sys-

<sup>1</sup> Harvard-Smithsonian Center for Astrophysics, Cambridge, MA 02138 USA; email: abieryla@cfa.harvard.edu

<sup>2</sup> Department of Physics and Astronomy, University of Louisville, Louisville, KY 40292, USA

<sup>3</sup> Department of Astronomy and Astrophysics, Pennsylvania State University, University Park, PA 16801, USA

<sup>4</sup> Las Cumbres Observatory Global Telescope Network, 6740 Cortona Drive, Suite 102, Santa Barbara, CA 93117, USA

<sup>5</sup> Department of Physics and Astronomy, Vanderbilt University, Nashville, TN 37235, USA

<sup>6</sup> Department of Physics, Lehigh University, Bethlehem, PA 18015, USA

<sup>7</sup> Department of Astronomy, The Ohio State University, 140 W. 18th Ave., Columbus, OH 43210, USA

<sup>8</sup> Department of Physics, Fisk University, Nashville, TN 37208, USA

<sup>9</sup> Niels Bohr Institute, University of Copenhagen, DK-2100, Denmark, and Centre for Star and Planet Formation, Natural History Museum of Denmark, DK-1350 Copenhagen

<sup>10</sup> Department of Astronomy, University of California Berkeley, Berkeley, CA 94720, USA

<sup>11</sup> NASA Sagan Fellow

<sup>12</sup> Department of Physics and Kavli Institute for Astrophysics and Space Research, Massachusetts Institute of Technology, Cambridge, MA 02139, USA

<sup>13</sup> Department of Physics and Astronomy, Swarthmore College, Swarthmore, PA 19081, USA

<sup>14</sup> Wellesley College, Wellesley, MA 02481, USA

<sup>15</sup> Atalaia Group and Crow-Observatory, Portalegre, Portugal

<sup>16</sup> Westminster College, New Wilmington, PA 16172, USA

<sup>17</sup> Institute of Astronomy, University of Hawaii at Manoa, 2680 Woodlawn Drive, Honolulu, HI 96822, USA

<sup>18</sup> National Science Foundation Graduate Research Fellow

<sup>19</sup> Yale University, New Haven, CT 06520, USA

<sup>20</sup> George P. and Cynthia Woods Mitchell Institute for Fundamental Physics and Astronomy, Texas A and M University, College Station, TX 77843-4242, USA

<sup>21</sup> Winer Observaotry, Sonoita, AZ 85637, USA

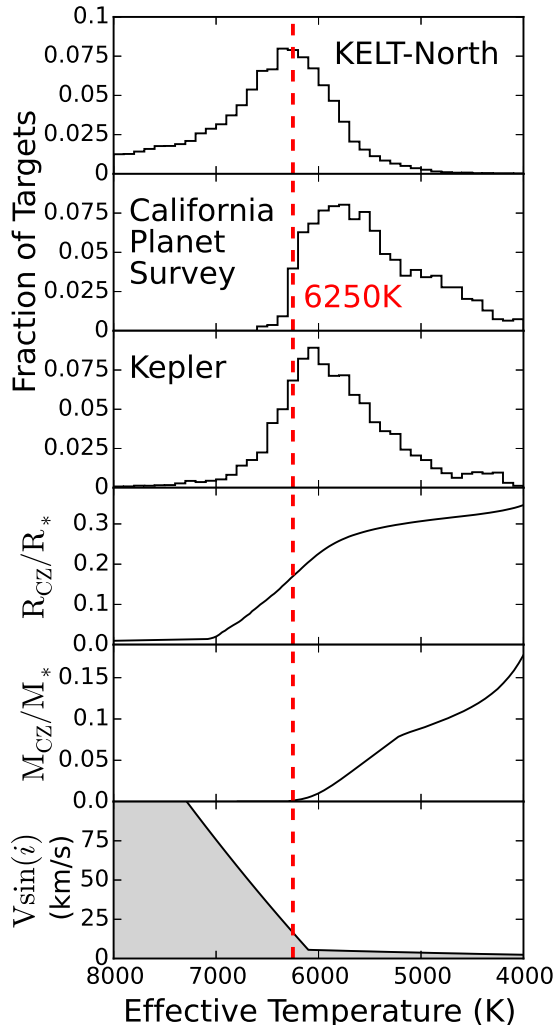


**Figure 1.** The top three panels show the effective temperature distribution for the stars targeted by the KELT-North transit survey (Sivard et al. 2012), the California Planet Survey (CPS) radial velocity (RV) search (Wright et al. 2004), and the Kepler mission (stars observed for all 16 quarters and with  $\log g > 4.0$  according to Kepler Q1-Q16 Stellar Parameters Database <sup>a</sup>). The fourth and fifth panels from the top show the relative depth and mass of outer stellar convective zones at these temperatures (van Saders & Pinsonneault 2012), while the sixth, bottom, panel shows the observed stellar  $v \sin i$  distribution (Reiners & Schmitt 2003). The red dashed line at 6250K shows the approximate location of the Kraft Break (Kraft 1970).

<sup>a</sup><http://exoplanetarchive.ipac.caltech.edu>, NASA Exoplanet Archive

tem. KELT-3b (Pepper et al. 2013) is a hot Jupiter transiting a  $V = 9.8$  slightly evolved late F-star. KELT-6b (Collins et al. 2014) is a mildly-inflated Saturn-mass planet transiting a metal poor, slightly evolved late F-star.

Because of its brighter magnitude range, the sample of host stars surveyed by KELT has a higher percentage of luminous stars than most transit surveys. This luminous subsample includes giants, as well as hot main-sequence stars and subgiants. Indeed, all five of the KELT-N discoveries to date (including KELT-7b) orbit F stars with  $T_{\text{eff}} > 6100\text{K}$ . Such hot stars are typically avoided by

radial velocity surveys. There is a transition between slowly and rapidly rotating stars known as the Kraft break (Kraft 1970, 1967). Stars hotter than the Kraft break around  $T_{\text{eff}} = 6250\text{K}$  typically have higher rotation velocities, making precision radial velocities more difficult. These higher rotation velocities reflect the angular momentum from formation, which is conserved as the stars evolve due to the lack of convective envelope. The lack of a convective envelope results in weak magnetic fields and ineffective magnetic braking from stellar winds (e.g., van Saders & Pinsonneault (2013)).

These points are illustrated in Figure 1, which shows the distribution of effective temperatures for the KELT stellar sample, the sample of stars targeted by Kepler, and a representative radial velocity survey. The KELT-North targets plotted here are all of the bright ( $V < 11$ ) putative dwarf stars in the survey which were selected by a reduced proper motion cut and with temperatures calculated from their J-K colors. Approximately 40,000 KELT-North targets are hotter than 6250K, 28 of the CPS targets are hotter than 6250K, and approximately 20,000 of the Kepler targets are hotter than 6250K. Also shown are theoretical estimates of the mass and radius of the convective envelope as a function of  $T_{\text{eff}}$  for stars with solar metallicity and an age of 1 Gyr (van Saders & Pinsonneault 2012), as well as the upper envelope of observed rotation velocities as a function of  $T_{\text{eff}}$  based from Reiners & Schmitt (2003).

Hot stars pose both opportunities and challenges for transit surveys. On the one hand, hot stars, particularly those with  $T_{\text{eff}} > 6500\text{K}$  and masses  $M > 1.5M_{\odot}$  have been relatively unexplored as compared to later spectral types. The first transiting planet was discovered by radial velocity surveys (Charbonneau et al. 2000; Henry et al. 2000), which initially targeted only late F, G, and early K stars. Due to the magnitude range of the stars surveyed and the choice of which candidates to follow up, the first dedicated ground-based transit surveys (Alonso et al. 2004; McCullough et al. 2006; Bakos et al. 2007; Collier Cameron et al. 2007) were also primarily sensitive to late F, G, and early K stars. As the value of transiting planets orbiting later stellar types was increasingly recognized, transit surveys began to survey lower-mass stars. Kepler extended the magnitude range of their target sample to fainter magnitudes (Gould et al. 2003; Batalha et al. 2010), in order to include a significant number of M dwarfs. The Kepler K2 mission will likely survey an even larger number of M stars than the prime mission (Howell et al. 2014). MEarth is specifically targeting a sample of some 3,000 mid to late M dwarfs (Irwin et al. 2014). Finally, HAT-South is surveying even fainter stars than HATNet, in order to increase the fraction of late G, K, and even early M stars (Bakos et al. 2013).

As a result of this focus on later spectral types, the population of close-in, low-mass companions to hot stars is relatively poorly assayed. For example, only 4 transiting planetary companions are known orbiting stars with  $T_{\text{eff}} > 6500\text{K}$  and  $M > 1.5M_{\odot}$ . Building a larger sample is particularly important given evidence that the population of planetary and substellar companions to hot and/or massive stars is significantly different than that of cooler and less massive stars. In particular, hot Jupiters orbiting hot ( $T_{\text{eff}} > 6250\text{K}$ ) stars tend to have a large

range of obliquities (Winn et al. 2010; Schlaufman 2010; Albrecht et al. 2012). There is evidence based on surveys of giant stars, whose progenitors are likely to be massive, hot stars (Johnson et al. (2013), but see Lloyd (2013)), that the distribution of Jovian planetary companions is a strong function of primary mass (Bowler et al. 2010). Finally, there is anecdotal evidence that massive substellar companions are more common around stars with  $T_{\text{eff}} > \sim 6200\text{K}$  (Bouchy et al. 2011).

The challenges posed by hot stars are primarily due to the high rotation velocities. The large rotation velocities of hot stars result in broad and weak lines, making precision radial velocity difficult. As a result, radial velocity surveys, and to a lesser extent transit surveys, have avoided targeting, or following up candidates from, such stars. Furthermore, for a fixed planet radius, the depths of planetary transits of hotter stars are shallower. This is exacerbated by the fact that stars with  $T_{\text{eff}} > 6500\text{K}$  have lifetimes that are of order the age of the Galactic disk, and thus tend to be significantly evolved.

However, there are a number of ways in which these challenges are mitigated for transit surveys. First, even though the transit depths are shallower, they are nevertheless greater than a few millimagnitudes, and thus readily detectable for Jovian-sized companions. Therefore, identifying such candidate transit signals is possible even for main-sequence stars as hot as  $7000\text{K}$ . Once a candidate signal is identified, its period can be confirmed with photometric follow-up. With a robust ephemeris in hand, radial velocity follow-up is greatly eased, as one is simply looking for a reflex variation with a specific period and phase (as opposed to searching over a wide range of these parameters, which increases the probability of false positives). Even with the relatively poor precision (a few  $100 \text{ m s}^{-1}$ ) of radial velocity measurements of hot stars, it is possible to exclude stellar companions and detect the reflex motion of relatively massive planetary and substellar companions.

Ultimately, however, it is precisely the high rotation velocities of hot stars that assist in robust confirmation of planetary transits, via the Rossiter-McLaughlin effect (RM) (Rossiter 1924; McLaughlin 1924). The rotating host star allows one to measure the spectral aberration of the absorption lines due to the small blockage of light as the planet transits the rapidly rotating host. The magnitude of this effect can be directly predicted by the rotation velocity measured from the spectrum, combined with the transit depth and shape. The RM effect can therefore provide strong confirmation that the transit signal is due to a planetary-sized object transiting the target star. However, for Jupiter-sized companions, this does not necessarily confirm the planetary nature of the occultor, because low-mass stars, brown dwarfs, and Jovian planets all have roughly  $\sim R_J$  (Chabrier & Baraffe 2000). However, even a crude upper limit on the Doppler amplitude of a few  $\text{km s}^{-1}$  can then be used to exclude essentially all companions with masses in the stellar or brown dwarf regime. Thus, the Doppler upper limit, combined with the RM measurement, essentially confirms that the companion is a planet, i.e. that is both mass and radius are in the planetary regime. Furthermore, the shape of the RM signal allows one to measure the projected angle between the planet's orbital axis and the star's rotation

axis. This projected obliquity provides clues to the formation and evolution (Albrecht et al. 2012) history of hot Jupiters and substellar companions. This effect also provides an independent measurement of the rotational velocity of the star.

In this paper, we describe the discovery and confirmation of a hot Jupiter transiting the bright  $V = 8.54$  star HD 33643, which we designate as KELT-7b. KELT-7 is a hot ( $\sim 6800 \text{ K}$ ), rapidly-rotating ( $v \sin i \sim 73 \text{ km s}^{-1}$ ) star, and its planetary companion was originally confirmed via the RM effect, which was easily detected with an amplitude of several hundred  $\text{m s}^{-1}$ . On the other hand, the reflex radial velocity motion of the star due to the companion was much more difficult to detect, although we did ultimately detect the signal at high confidence. This discovery therefore illustrates both the opportunities and challenges associated with confirming planetary companions transiting hot stars. We note that, because of its brighter magnitude range, the Transiting Exoplanet Survey Satellite (TESS) (Ricker et al. 2014) will also survey a large number of hot stars. Therefore, at least some of the lessons learned from KELT for characterizing the population of planets orbiting hot stars are likely to apply to TESS as well.

## 2. DISCOVERY AND FOLLOW-UP OBSERVATIONS

The KELT-N survey has a standard process of data reduction which will be briefly described in Section 2.1. For more information see Siverd et al. (2012).

### 2.1. KELT Observations and Photometry

KELT-7 is in KELT-N survey field 04, which is centered on ( $\alpha = 05h:54m:14.71s$ ,  $\delta = +31d:39m:55.10s$ ;  $J2000$ ). Field 04 was monitored from 2006 October 26 to 2011 April 1 collecting about 7800 images. The KELT-7 light curve in particular had 7745 points after a single round of iterative  $3\sigma$  outlier clipping that occurs just after the trend filtering algorithm (TFA) (Kovács et al. 2005). We reduced the raw survey data using a custom implementation of the ISIS image subtraction package (Alard & Lupton 1998; Alard 2000), combined with point-spread-function photometry using DAOPHOT (Stetson 1987). Using proper motions from the Tycho-2 catalog (Høg et al. 2000) and  $J$  and  $H$  magnitudes from 2MASS (Skrutskie et al. 2006; Cutri et al. 2003), we applied a reduced proper motion cut (Gould et al. 2003) based on the implementation of Collier Cameron et al. (2007). This allowed us to select likely dwarf and subgiant stars within the field for further post-processing and analysis. We applied the TFA to each selected light curve to remove systematic noise, followed by a search for transit signals using the box-fitting least squares algorithm (BLS) (Kovács et al. 2002). For both TFA and BLS we used the versions found in the VARTOOLS package (Hartman et al. 2008).

One of the candidates from field 04 was star HD 33643 / 2MASS 05131092+3319054 / TYC 2393-852-1, located at ( $\alpha = 05h:13m:10.93s$ ,  $\delta = +33d:19m:05.40s$ ;  $J2000$ ). The star has Tycho magnitudes  $B_T = 9.074$  and  $V_T = 8.612$  (Høg et al. 2000) and passed our initial selection cuts. The discovery light curve of KELT-7 is shown in Figure 2. We observed a transit-like feature at a period of 2.7347749 days, with a depth of about 8.28 mmag.

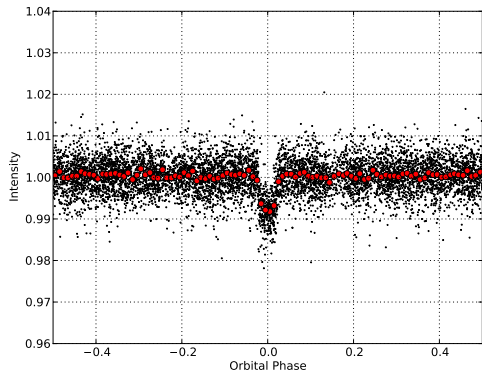


**Figure 2.** Discovery light curve of KELT-7b from the KELT-N telescope. The light curve contains 7745 observations spanning 4.5 years, phase folded to the orbital period of  $P = 2.7347749$  days. The red line represents the same data binned at 1 hr intervals in phase.

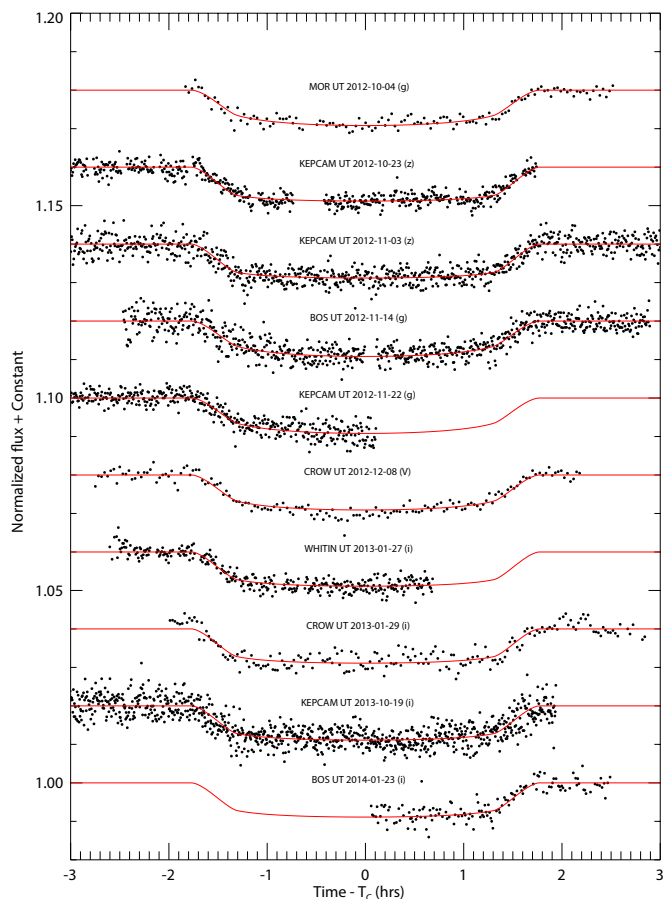


**Figure 3.** Follow-up transit photometry of KELT-7. The red overplotted line is the best fit transit model. The labels are as follows: MOR=University of Louisville Moore Observatory; KEPCAM=KeplerCam at the Fred Lawrence Whipple Observatory; BOS=Bryne Observatory at Sedgwick (LCOGT); CROW=Canela’s Robotic Observatory; WHITIN=Whitin Observatory at Wellesley College

## 2.2. Follow-up Time Series Photometry

We obtained follow-up time-series photometry of KELT-7 to check for false positives and better determine the transit shape. We used the Tapir software package (Jensen 2013) to predict transit events, and we obtained

10 full or partial transits in multiple bands between October 2012 and January 2014. All data were calibrated and processed using the AstroImageJ package<sup>22</sup> (AIJ; K. Collins et al., in prep.) unless otherwise stated.

We obtained one full transit of KELT-7b in the  $g$ -band on UT2012-10-04 at the University of Louisville’s Moore Observatory. We used the 0.6 m RC Optical Systems (RCOS) telescope with an Apogee U16M 4K x 4K CCD, giving a  $26' \times 26'$  field of view and  $0.39$  arcsec pixel<sup>-1</sup>.

We used KeplerCam on the 1.2 m telescope at the Fred Lawrence Whipple Observatory (FLWO) to observe two full  $z$ -band transits on UT2012-10-23 and on UT2012-11-03. We also observed a partial  $g$ -band transit on UT2012-11-22. On the night of UT2013-10-19 we observed a full  $i$ -band transit in combination with radial velocity observations to measure the RM effect (described more in Section 2.4). KeplerCam has a single 4K x 4K Fairchild CCD with  $0.366$  arcsec pixel<sup>-1</sup> and a field of view of  $23.1' \times 23.1'$ . The data were reduced using procedures outlined in Carter et al. (2011), which uses standard IDL routines.

We observed a full transit in  $g$ -band on UT2012-11-14 and a partial transit in  $i$ -band on UT2014-01-23 from the Byrne Observatory at Sedwick (BOS), operated by Las Cumbres Observatory Global Telescope (LCOGT). BOS is a 0.8 m RCOS telescope with a 3K x 2K SBIG STL-6303E detector. It has a  $14.7' \times 9.8'$  field of view and  $0.572$  arcsec pixel<sup>-1</sup>. Data on the night of UT2012-11-14 were reduced and light curves were extracted using standard IRAF/PyRAF routines as described in Fulton et al. (2011). Observations from UT2014-01-23 were analyzed using custom routines written in GDL.<sup>23</sup>

We observed two full transits at Canela’s Robotic Observatory (CROW) in Portugal. Observations were made using the 0.3 m LX200 telescope with a SBIG ST-8XME CCD. The field of view is  $28' \times 19'$  and  $1.11$  arcsec pixel<sup>-1</sup>. Observations were taken on UT2012-12-08 and UT2013-01-29 in  $V$ -band and  $i$ -band, respectively.

We observed one partial transit in  $I$ -band on the night of UT2013-01-27 at the Whitin Observatory at Wellesley College. The observatory uses a 0.6 m Boller and Chivens telescope with a DFM focal reducer that gives an effective focal ratio of  $f/9.6$ . The camera is an Apogee U230 2K x 2K with a  $0.58$  arcsec pixel<sup>-1</sup> scale and a  $20' \times 20'$  FOV. Reductions were carried out using standard IRAF packages, with photometry done in AIJ.

Figure 3 shows each transit plotted with the best fit transit model overplotted in red. Figure 4 shows the combined and binned light curve with all 10 transits.

## 2.3. Spectroscopic Observations

We used the Tillinghast Reflector Echelle Spectrograph (TRES; Fúresz 2008), on the 1.5 m telescope at the Fred Lawrence Whipple Observatory (FLWO) on Mt. Hopkins, Arizona, to obtain spectra to test false positive scenarios, characterize radial velocity (RV) variations and determine stellar parameters of the host star. We obtained a total of 64 TRES spectra between UT 2012 January 31 and UT 2014 February 21. The spectra have a

<sup>22</sup> <http://www.astro.louisville.edu/software/astroimagej>

<sup>23</sup> GNU Data Language; <http://gnudatalanguage.sourceforge.net/>

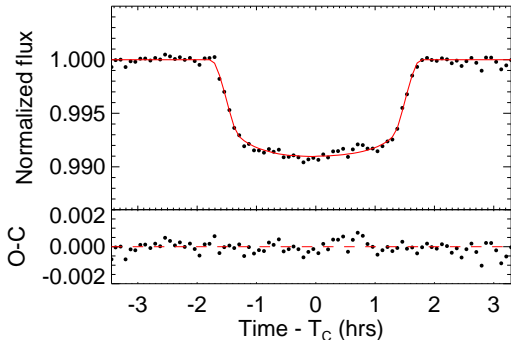


**Figure 4.** Top panel: All follow-up light curves from Figure 3, combined and binned in 5 minute intervals. This light curve is not used for analysis, but is shown in order to illustrate the best combined behavior of the light curve data set. The red curve shows the 10 transit models for each of the individual fits combined and binned in 5 minute intervals the same way as the data, with the model points connected. Bottom panel: The residuals of the binned light curve from the binned model in the top panel.

resolving power of  $R = 44,000$  and were extracted as described by Buchhave et al. (2010).

Initially we obtained observations near phases 0.25 and 0.75 in order to check for large velocity variations due to a small stellar companion responsible for the light curve. The spectrum appeared to be single-lined, and the velocity variation that we saw was much too small to be due to a stellar companion so we continued observing to get a preliminary orbit. The orbit had a fair amount of scatter due to the rapid rotation of the host star so we stopped observing spectroscopically and opted instead to follow-up the star photometrically to confirm the depth, shape, and period of the transit, and to search for color-depth dependent depth variations indicative of a blended eclipsing binary.

Once we had observed multiple transits in different filters to determine that the transit depths were indeed achromatic, we started obtaining high signal-to-noise ratio spectra to refine the orbit and to determine stellar parameters of the host star. Of the 64 total spectra, 28 were taken on the night of UT 2013 October 19 to measure the RM effect (see Section 2.4). Table 1 lists all of the RV data for Kelt-7.

#### 2.4. Rossiter-McLaughlin Observations

We observed the RM effect on the night of UT 2013 October 19 to determine the projected obliquity of the system. Simultaneous data were taken using the TRES spectrograph on the 1.5 m telescope and photometric data using KeplerCam on the 1.2 m telescope both atop Mt. Hopkins in AZ. We collected 28 RV spectra with a 15 minute exposure cadence and signal-to-noise ratio ranging from 127 to 165 per resolution element. For the spectroscopic observations we began collecting data an hour and a half before ingress but we only obtained 2 observations after egress due to morning twilight. Photometric observations were gathered starting two hours prior to ingress until morning twilight which occurred about 10 minutes after egress. We obtained a total of 997 KeplerCam observations at an exposure time of 2 seconds and a slight defocus of the image because of the brightness of the star.

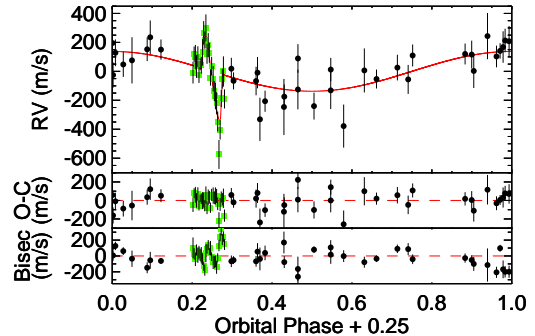


**Figure 5.** TRES radial velocities of Kelt-7. The green squares represent data taken on the night of the RM event, while the black circles are data that were not taken during transit. The phases have been shifted so that a phase of 0.25 corresponds to the time of the primary transit,  $T_C$ . Top panel: RV observations phased to zero and with no linear trend, shown in red. The predicted RM effect in the model shown incorporates the best fit model where  $\lambda = 9.7 \pm 5.2$  degrees. Middle panel: Residuals of the RV observations to our circular orbital fit. Bottom panel: Bisector span of the RV observations as a function of phase.

#### 2.5. Adaptive Optics Observations

We obtained adaptive optics (AO) imagery for Kelt-7 on UT 2014 August 17 using the NIRC2 (instrument PI: Keith Matthews) with the Keck II Natural Guide Star (NGS) AO system (Wizinowich 2000). We used the narrow camera setting with a plate scale of 10 mas  $\text{pixel}^{-1}$ . The setting provides a fine spatial sampling of the instrument point spread function (PSF). The observing conditions were good, with seeing of  $0.5''$ . Kelt-7 was observed at an airmass of 1.31. We used a Br- $\gamma$  filter to acquire images with a 3-point dither method. At each dither position, we took an exposure of 0.5 second per coadd and 20 coadds. The total on-source integration time was 30 sec.

The raw NIRC2 data were processed using standard techniques to replace bad pixels, flat-field, subtract thermal background, align and co-add frames. We did not find any nearby companions or background sources at the  $5\text{-}\sigma$  level (Fig. 6). We calculated the  $5\text{-}\sigma$  detection limit as follows. We defined a series of concentric annuli centered on the star. For the concentric annuli, we calculated the median and the standard deviation of flux for pixels within these annuli. We used the value of five times the standard deviation above the median as the  $5\text{-}\sigma$  detection limit. The  $5\text{-}\sigma$  detection limits are  $\Delta\text{mag}=2.5$  mag, 5.4 mag, 6.4 mag, and 7.3 mag for  $0.1''$ ,  $0.2''$ ,  $0.5''$ , and  $1.0''$ , respectively.

### 3. ANALYSIS

#### 3.1. Spectroscopic Analysis

Using the Spectral Parameter Classification (SPC) (Buchhave et al. 2012) technique, with  $T_{\text{eff}}$ ,  $\log g$ ,  $[\text{m}/\text{H}]$ , and  $v \sin i$  as free parameters, we obtained stellar parameters of Kelt-7 from the 64 TRES spectra. SPC cross correlates an observed spectrum against a grid of synthetic spectra based on Kurucz atmospheric models (Kurucz 1992). The values were calculated using a weighted mean, taking into account the cross-correlation function (CCF) peak height. The weighted average results are:  $T_{\text{eff}} = 6779 \pm 50$  K,  $\log g = 4.23 \pm 0.10$ ,  $[\text{m}/\text{H}] =$



**Table 1**  
RV Observations of KELT-7

Time <i>BJD<sub>TDB</sub></i>	Relative RV ( $\text{m s}^{-1}$ )	Relative RV error ( $\text{m s}^{-1}$ )	Bisector ( $\text{m s}^{-1}$ )	Bisector error ( $\text{m s}^{-1}$ )	Phase	SNRe <sup>a</sup>
2455957.836103	102	143	-114	209	-0.3053	68.8
2455961.748540	-472	134	-37	143	1.1253	87.4
2455963.607625	-65	144	-35	102	1.8050	122.7
2455964.647614	-387	174	170	137	2.1853	82.2
2455967.702756	-129	73	16	116	3.3024	101.0
2455968.667152	-25	86	-52	61	3.6551	191.2
2455970.667266	-135	136	-79	69	4.3864	106.3
2455971.657526	67	95	-199	77	4.7485	161.3
2455982.637552	-13	83	127	53	8.7633	153.3
2455983.610040	-150	97	55	107	9.1189	174.2
2455984.641133	-197	90	86	76	9.4959	180.2
2455985.610681	94	104	-55	107	9.8504	122.0
2455986.621278	-267	123	-164	156	10.2200	92.1
2456019.663088	-273	115	108	92	22.3017	73.5
2456020.642102	-139	107	-100	88	22.6597	125.5
2456027.643080	-52	89	-262	119	25.2196	141.2
2456310.790708	55	117	144	60	128.7524	296.9
2456340.790829	0	48	97	44	139.7219	297.5
2456584.819001	-45	88	102	131	228.9507	131.4
2456584.826693	81	64	26	71	228.9535	127.1
2456584.835357	62	100	-42	85	228.9567	146.6
2456584.843054	-1	93	75	70	228.9595	148.1
2456584.852250	65	85	8	95	228.9629	144.0
2456584.859959	-62	63	41	87	228.9657	144.5
2456584.867813	13	48	14	78	228.9686	145.7
2456584.875811	7	68	8	104	228.9715	143.5
2456584.884423	96	108	-39	74	228.9746	154.8
2456584.892300	230	96	-130	57	228.9775	154.3
2456584.899864	181	71	-179	70	228.9803	155.7
2456584.907399	265	110	33	112	228.9830	161.2
2456584.915097	86	82	89	61	228.9858	155.4
2456584.923361	146	98	138	62	228.9889	154.1
2456584.930798	93	81	56	43	228.9916	153.1
2456584.938490	-78	65	98	91	228.9944	162.9
2456584.946413	1	76	-9	55	228.9973	162.7
2456584.956825	-87	103	-80	84	229.0011	161.8
2456584.964968	-172	82	-77	78	229.0041	166.5
2456584.972520	-205	109	-70	74	229.0068	165.2
2456584.980362	-255	89	-143	82	229.0097	158.9
2456584.987938	-382	80	-23	56	229.0125	164.0
2456584.996897	-610	118	132	72	229.0158	162.3
2456585.004641	-437	81	240	53	229.0186	165.4
2456585.012118	-223	70	336	79	229.0213	162.9
2456585.019665	-86	80	207	70	229.0241	159.9
2456585.027143	-37	123	243	65	229.0268	156.1
2456585.034609	-226	78	145	70	229.0295	156.2
2456638.901881	26	98	-169	112	248.7261	198.1
2456639.777025	-123	68	-67	73	249.0461	242.0
2456640.913299	-115	80	90	53	249.4616	262.4
2456641.702340	-166	78	6	67	249.7501	169.0
2456642.742449	-347	66	39	92	250.1304	258.3
2456693.611029	72	73	-200	72	268.7305	203.3
2456694.641506	-208	89	-67	68	269.1073	186.2
2456696.631120	11	73	-149	70	269.8348	229.6
2456700.710497	-519	134	-2	75	271.3264	146.0
2456701.756533	-38	67	-206	70	271.7089	238.9
2456702.691941	-207	53	-53	50	272.0509	278.9
2456703.670164	-194	59	-35	42	272.4086	263.7
2456704.671919	-94	77	61	50	272.7749	219.1
2456705.773764	-316	76	-78	75	273.1778	220.1
2456706.652092	-32	68	-41	60	273.4989	254.3
2456707.664631	9	63	-63	37	273.8692	238.4
2456708.711942	-381	84	80	42	274.2521	206.1
2456709.746023	-21	65	-27	59	274.6302	260.8

<sup>a</sup> Signal to noise per resolution element (SNRe) which takes into account the resolution of the instrument. SNRe is calculated near the peak of the echelle order that includes the Mg b lines.

**Table 2**  
Stellar Properties of KELT-7

Parameter	Description	Value	Source	Reference <sup>a</sup>
Names		BD +33 977 TYC 2393-852-1 2MASS 05131092+3319054 GSC 2393-00852 HD 33643		
$\alpha_{J2000}$		05 13 10.93	Tycho-2	1
$\delta_{J2000}$		+33 19 05.40	Tycho-2	1
$NUV_{GALEX}$		$13.330 \pm 0.905$	GALEX	2
$B_T$		$9.074 \pm 0.030$	Tycho-2	1
$V_T$		$8.612 \pm 0.030$	Tycho-2	1
$V$		$8.540 \pm 0.030$	SKY2000	3
$B$		$8.970 \pm 0.030$	SKY2000	3
$U$		$9.010 \pm 0.030$	SKY2000	3
$I_C$		$8.129 \pm 0.051$	TASS	4
$J$		$7.739 \pm 0.030$	2MASS	5
$H$		$7.580 \pm 0.042$	2MASS	5
$K$		$7.543 \pm 0.030$	2MASS	5
$WISE1$		$10.179 \pm 0.050$	WISE	6
$WISE2$		$10.844 \pm 0.050$	WISE	6
$WISE3$		$12.766 \pm 0.180$	WISE	6
$WISE4$		$13.741 \pm 0.123$	WISE	6
$\mu_\alpha$	Proper Motion in RA (mas yr <sup>-1</sup> )	$10.40 \pm 0.70$	UCAC4	7
$\mu_\delta$	Proper Motion in DEC (mas yr <sup>-1</sup> )	$-49.70 \pm 0.60$	UCAC4	7
$U^b$	km s <sup>-1</sup>	$-33.5 \pm 0.2$	This paper	
$V$	km s <sup>-1</sup>	$-9.7 \pm 1.8$	This paper	
$W$	km s <sup>-1</sup>	$-8.4 \pm 0.9$	This paper	
$d$	Distance (pc)	$129 \pm 8$	This paper	
	Age (Gyr)	$1.3 \pm 0.2$	This paper	
$A_V$	Visual extinction	$0.13 \pm 0.04$	This paper	

<sup>a</sup> References: (1)Høg et al. (2000); (2)Martin et al. (2005); (3)Myers et al. (2001); (4)Richmond et al. (2000); (5)Cutri et al. (2003); Skrutskie et al. (2006); (6)Wright et al. (2010); Cutri & et al. (2012); (7)Zacharias et al. (2013)

<sup>b</sup> Positive U is in the direction of the Galactic center.

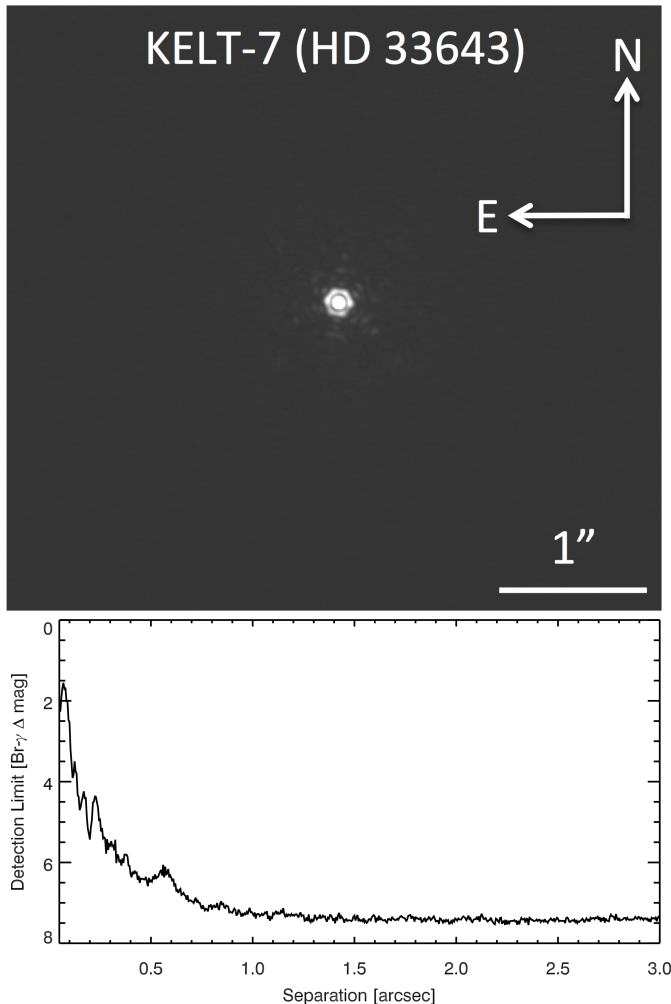


**Figure 6.** Top: Br- $\gamma$  AO image for KELT-7 (HD 33643) in Br- $\gamma$  ( $\lambda = 2.1654 \mu\text{m}$ ). North is up, east is left. The horizontal bar is  $1''$ . No nearby companions or background sources were detected. Bottom:  $5\sigma$  detection limit as a function of angular separation. Detection limits at  $0.1''$ ,  $0.2''$ ,  $0.5''$ , and  $1.0''$  are also given in Section 2.5.

$0.12 \pm 0.08$ , and  $v \sin i = 73.2 \pm 0.5 \text{ km s}^{-1}$ .  $[\text{m}/\text{H}]$  was substituted for  $[\text{Fe}/\text{H}]$  in this analysis but we do not believe that this will affect the results.<sup>24</sup>

Figure 5 shows the best-fit orbit and computed bisectors with residuals. The relative RVs were derived by cross-correlating the spectra against the strongest observed spectrum from the wavelength range  $4250 - 5650 \text{ \AA}$ . The bisector analysis of the RVs taken out of transit showed no indication that the bisector spans were in phase with the photometric ephemeris but the RMS was large due to the high  $v \sin i$ . Despite the higher  $v \sin i$  and resulting poorer precision, we were ultimately able to detect the reflex signal at high confidence (roughly  $7\sigma$ ). We do see a correlation between the bisectors and RVs taken during the transit due to the RM effect. The

<sup>24</sup> SPC compares the observed spectra against a library of synthetic spectra calculated with the same mix of metals as the Sun. Since it uses all the lines in the observed spectra in the wavelength region covered by the library, the metallicity  $[\text{m}/\text{H}]$  is the same as  $[\text{Fe}/\text{H}]$  only if the mix of metals in the target star is the same as the Sun.

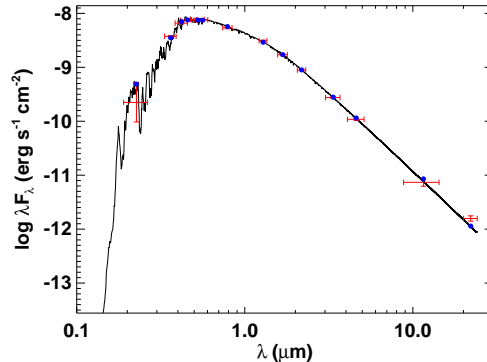


**Figure 7.** Measured and best-fit SED for KELT-7 from UV through mid-IR. The red error bars indicate measurements of the flux of KELT-7 in UV, optical, NIR, and mid-IR passbands and listed in Table 2. The vertical bars are the  $1\sigma$  photometric uncertainties, whereas the horizontal error bars are the effective widths of the passbands. The solid curve is the best-fit theoretical SED from the NextGen models of Hauschildt et al. (1999), assuming stellar parameters  $T_{\text{eff}}$ ,  $\log g$ , and  $[\text{Fe}/\text{H}]$  fixed at the adopted values in Table 4, with  $A_V$  and  $d$  allowed to vary. The blue dots are the predicted passband-integrated fluxes of the best-fit theoretical SED corresponding to our observed photometric bands. The  $22 \mu\text{m}$  band shows a slight IR excess as discussed in Section 3.3.

relative RVs and bisector values are listed in Table 1.

### 3.2. UVW Space Motion

We evaluate the motion of KELT-7 through the Galaxy to place it among standard stellar populations. The absolute heliocentric radial velocity is  $+39.4 \pm 0.1 \text{ km s}^{-1}$ , where the uncertainty is due to the systematic uncertainties in the absolute velocities of the RV standard stars. Combining the absolute TRES RV with the distance from the spectral energy distribution analysis and proper motion information from the UCAC4 catalog (Zacharias et al. 2013), we find that KELT-7 has a  $U, V, W$  (where positive  $U$  is the direction of the Galactic center) of  $-33.5 \pm 0.2, -9.7 \pm 1.8, -8.4 \pm 0.9$ , all in units of  $\text{km s}^{-1}$ , making this a thin disk star (Bensby et al. 2003).

### 3.3. SED Analysis

We construct an empirical spectral energy distribution (SED) of KELT-7 shown in Figure 7. We use the near-UV bandpasses from GALEX (Martin et al. 2005), the  $B_T$  and  $V_T$  colors from the *Tycho-2* catalog (Høg et al. 2000), near-infrared (NIR) fluxes in the  $J$  and  $H$  passbands from the 2MASS Point Source Catalog (Cutri et al. 2003; Skrutskie et al. 2006), and near- and mid-infrared fluxes in the four *WISE* passbands (Wright et al. 2010) to derive the SED. We fit this SED to the NextGen models from Hauschildt et al. (1999) by fixing the values of  $T_{\text{eff}}$ ,  $\log g$ , and  $[\text{Fe}/\text{H}]$  inferred from the global fit to the light curve and RV data as described in Section 3.7 and listed in Table 4, and then finding the values of the visual extinction  $A_V$  and distance  $d$  that minimize  $\chi^2$ . We find  $A_V = 0.13 \pm 0.04$  and  $d = 129 \pm 8 \text{ pc}$  with the best fit model having a reduced  $\chi^2 = 1.83$ . We note that the quoted statistical uncertainties on  $A_V$  and  $d$  are likely to be underestimated because we have not accounted for the uncertainties in values of  $T_{\text{eff}}$ ,  $\log g$ , and  $[\text{Fe}/\text{H}]$  used to derive the model SED. Furthermore,



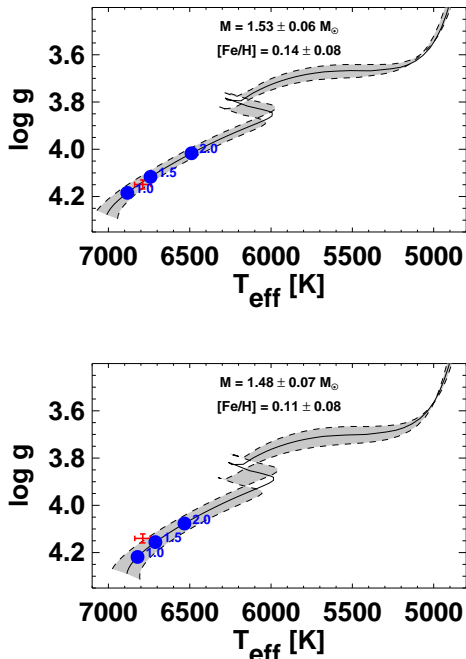


**Figure 8.** Theoretical HR diagrams based on Yonsei-Yale stellar evolution models (Demarque et al. 2004). The solid lines represent the evolutionary tracks for the best-fit values of the mass and metallicity of the host star from the global fits using the Yonsei-Yale constraints (top panel) and the Torres constraints (bottom panel) as described in Section 3.7. The tracks for the extreme range of  $1\sigma$  uncertainties on  $M_*$  and  $[\text{Fe}/\text{H}]$  are shown as dashed lines, bracketing the  $1\sigma$  range shown in grey. The red crosses show  $T_{\text{eff}}$  and  $\log g$  from the EXOFAST global fit analysis, the blue dots represent the location of the star for various ages in Gyr. We adopt the Yonsei-Yale constrained global fit represented in the top panel resulting in an estimated age of  $1.3 \pm 0.2$  Gyr, where we note the uncertainty does not include possible systematic errors in the adopted evolutionary tracks.

it is likely that alternate model atmospheres would predict somewhat different SEDs and thus values of extinction and distance.

Our SED analysis yields a slight IR excess in the 22 micron band which was also reported by McDonald et al. (2012) in a study of IR excess of Hipparcos stars. Due to the young age of this star (see Section 3.4), the detection of this excess could be evidence for a debris disk, though we suspect that it is likely due to background nebulosity. The star appears to lie in a region of considerably higher IR nebulosity than its surroundings.

### 3.4. Evolutionary Analysis

We use  $T_{\text{eff}}$ ,  $\log g$ , stellar mass, and metallicity derived from the EXOFAST global fits (see Section 3.7 and Table 4), in combination with the theoretical evolutionary tracks of the Yonsei-Yale stellar models (Demarque et al. 2004), to estimate the age of the KELT-7 system. We have not directly applied a prior on the age, but rather have assumed uniform priors on  $[\text{Fe}/\text{H}]$ ,  $\log g$ , and  $T_{\text{eff}}$ , which translates into non-uniform priors on the age. Figure 8 shows the theoretical HR diagram ( $\log g$  vs.  $T_{\text{eff}}$ ) with evolutionary tracks for masses corresponding to the  $\pm 1\sigma$  extrema in estimated uncertainty. We adopt the Yonsei-Yale constrained global fit represented in the top panel. We compare the intersection of the global fit val-

ues for  $T_{\text{eff}}$  and  $\log g$  and associated uncertainties to the evolutionary track to estimate the age of KELT-7. We estimate the age to be  $1.3 \pm 0.2$  Gyr. The bottom panel of Figure 8 is shown as a comparison using the Torres constrained global fit values (Torres et al. 2010). The Torres models provide empirical relationships between observed stellar parameters  $T_{\text{eff}}$ ,  $\log g$ , and  $[\text{Fe}/\text{H}]$ , and stellar mass and radius. The Torres values are consistent with the Yonsei-Yale model values within  $1\sigma$  and are shown in Table 4.

### 3.5. Rossiter-McLaughlin Analysis

We performed an analysis of the RM data separately from the global fit analysis (see Section 3.7). To model the RM effect, we used parameter estimation and model fitting protocols as described in Sanchis-Ojeda et al. (2013) and Albrecht et al. (2012). The code implements formulas from Hirano et al. (2011), using the loss of light calculated from transit parameters and planet position as inputs. The transit data from the night of the RM event were used to determine the time of transit and transit parameters  $b$ ,  $R_*/a$ ,  $R_p/R_*$ . Additional free parameters are  $v \sin i$  and  $\lambda$  to describe the amplitude and shape of the signal, and slope  $\dot{\gamma}$  and offset  $\gamma$  to describe the orbital motion of the star. The uncertainty of the model parameters were estimated using a Markov Chain Monte Carlo (MCMC) algorithm, where the number of chains was large enough to guarantee the robustness of the final values.

The results from the analysis show that the sky-projected obliquity is  $\lambda = 4.1^{+7.9}_{-7.7}$  degrees. The analysis also gives us an independent measure of the projected rotational velocity,  $v \sin i = 66^{+21}_{-19} \text{ km s}^{-1}$ , which is consistent with the SPC analysis (see Section 3.1). We can also use the result from the out of transit velocity  $\dot{\gamma} = -671^{+346}_{-340} \text{ m s}^{-1}$  to estimate the velocity semi-amplitude due to the planet. Using the orbital period and assuming a circular orbit, we calculate  $K_{RV} = 292 \pm 146 \text{ m s}^{-1}$ . This result is consistent with the  $K_{RV} = 138 \pm 19 \text{ m s}^{-1}$  value from the Doppler RV analysis (See Section 3.1). The results from this analysis are shown in Figure 9.

### 3.6. Time-series Spectral Line Profile

The overall starlight that is blocked by the planet during transit will appear as a bump in the rotational broadening function (Collier Cameron et al. 2010). Each spectrum taken on the night of the RM event was cross-correlated against a non-rotating template. The CCFs of the out-of-transit data were median combined to create a master OOT CCF. The master was then subtracted from all of the in- and out-of-transit CCFs. Figure 10 is a greyscale plot showing the results. The bright white feature increasing in velocity with time is caused by the planet as it transits the star. This feature is what we would expect to see for a system that has low orbital obliquity.

### 3.7. EXOFAST Global Fit

We used a custom version of EXOFAST (Eastman et al. 2013) to determine a global fit of the system. EXOFAST does a simultaneous MCMC analysis of the photometric and spectroscopic data, including constraints on the stellar parameters of  $M_*$  and  $R_*$  from

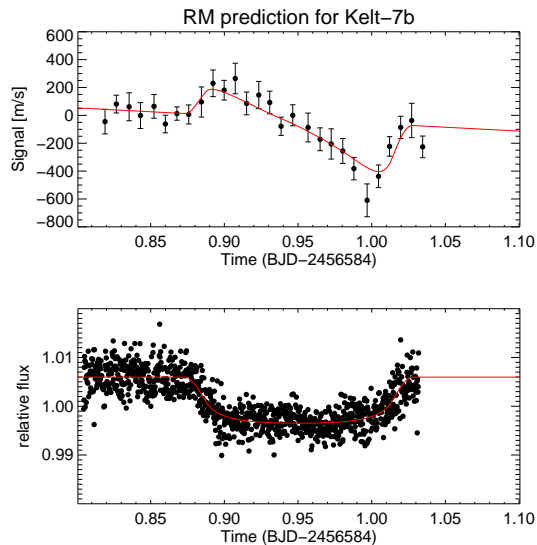


**Figure 9.** RM results from our independent analysis. Spectroscopic and photometric data are from UT2013 October 19. Top Panel: RV observations with the best RM fit shown in red. Bottom Panel: Photometric transit data with the best fit shown in red. Data are plotted in time for comparison.

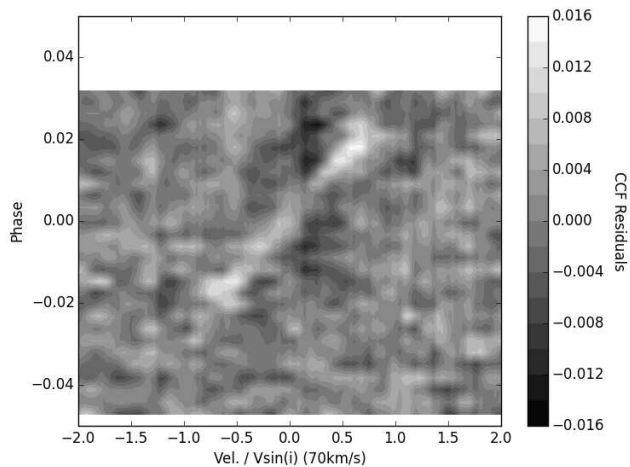


**Figure 10.** Time series of the residual average spectral line profile for data taken on UT2013 October 19. The bright white feature is caused by the planet transiting the star.

the empirical Torres relations (Torres et al. 2010) or Yonsei-Yale (YY) evolutionary models (Demarque et al. 2004), to derive system parameters. This method is similar to that described in detail in Siverd et al. (2012), but we note a few differences below <sup>25</sup>.

As initial inputs for EXOFAST we included as priors the orbital period  $P = 2.7347749 \pm 0.000004$  days from the KELT-N data and the host star effective temperature  $T_{\text{eff}} = 6779 \pm 50$  K, metallicity  $[m/H] = 0.12 \pm 0.08$ , and stellar surface gravity  $\log g = 4.23 \pm 0.10$  from TRES

<sup>25</sup> In the EXOFAST analysis, which includes the modeling of filter-specific limb darkening parameters of the transit, we employ the transmission curves defined for the primed SDSS filters rather than the unprimed versions. We expect any differences due to that discrepancy to be well below the precision of all our observations in this paper and of the limb darkening tables from Claret & Bloemen (2011).

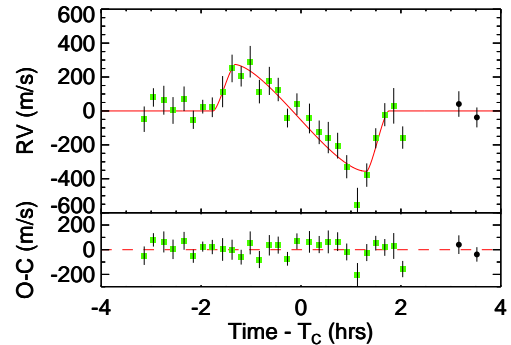


**Figure 11.** RM results from the global EXOFAST fit with the reflex velocity subtracted out. Top panel: RV data (green points) from UT 2013 October 19 with the best fit model shown in red. The two black points were taken on different nights and not included in the fit. The shape of the RM signal implies that the projected obliquity of the host star with respect to the planet is small. Bottom panel: The residuals of the data to the RM fit.

spectroscopy. The priors were implemented as a  $\chi^2$  penalty in EXOFAST (see Eastman et al. (2013) for details). In fitting the TRES RVs independently to a Keplerian model we did not detect a significant slope in the RVs (i.e., due to an additional long-period companion), and we therefore did not include this as a free parameter in our final fits.

We used the AIJ package to determine detrending parameters for the light curves, such as corrections for airmass and meridian flip. AIJ allows interactive detrending capabilities. Once we determined the detrending parameters for each light curve, we fit the transit light curves using EXOFAST. All light curves are detrended by airmass while the CROW light curve from UT2013 January 29 was also detrended by meridian flip and average FWHM in the image. The raw data with detrending parameters were used as the input for EXOFAST, and final detrending was done in EXOFAST.

There were a few other considerations when running the global fit. First, we had to choose whether to include just the full transits, with an ingress and an egress, or to include all transits including the partial transits that were missing an ingress or an egress. Second, we had the option of allowing the orbital eccentricity and argument of periastron to float free or to fix them to zero and force a circular orbit. Third, we had to choose between constraining the mass-radius relationship using the Torres relations or by using the Yonsei-Yale stellar models. Finally, we had the option to include the RM observations and fit the RM RVs as part of the global fit.

For the initial runs, we chose to use only the full transits and the non-RM RVs to ensure convergence. We also chose to fix the eccentricity to zero and set the constraint on the mass-radius relationship using the Torres relations. Once the fit converged, we ran it again but changed the constraint on the mass-radius relationship to the YY stellar models. We found the final parameters were in agreement within the uncertainties. This gave us confidence to start adding the partial transits. We initially had trouble getting the fit to converge with all the light curves and found that we needed to add prior width constraint on the transit timing variation (TTV) and the baseline flux for the partial transits. We then released the prior on eccentricity and let it float free. The result

**Table 3**  
Transit Times for KELT-7

Epoch	$T_C$ ( $BJD_{TDB}$ )	Error sec	O-C sec	O-C/Error	Observatory
-55	2456204.817057	64	5.65	0.09	MOR
-48	2456223.959470	31	-83.91	-2.70	KEPCAM
-44	2456234.898861	42	-59.97	-1.42	KEPCAM
-40	2456245.839584	50	79.05	1.56	BOS
-37	2456254.045118	63	182.60	2.88	KEPCAM
-31	2456270.451621	55	-4.72	-0.08	CROW
-13	2456319.678871	59	102.16	1.72	WHITIN
-12	2456322.413721	56	108.34	1.92	CROW
84	2456584.950978	47	-19.45	-0.41	KEPCAM
119	2456680.667558	87	-77.12	-0.88	BOS

was  $e = 0.013_{-0.010}^{+0.022}$  which was consistent with a circular orbit.

The last step of the process was to include the RM velocities in the combined global fit. The RM data were modeled using the Ohta et al. (2005) analytic approximation with linear limb darkening. At each step in the Markov Chain, we interpolated the linear limb darkening tables of Claret & Bloemen (2011) based on the chain’s value for  $\log g$ ,  $T_{\text{eff}}$ , and  $[\text{Fe}/\text{H}]$  to derive the linear limb darkening coefficient,  $u$ . The RM RVs were allowed a velocity offset ( $\gamma_{RM}$ ) separate from the non-RM RV dataset velocity zeropoint ( $\gamma$ ). We allowed for this because stars have intrinsic jitter (Albrecht et al. 2012; Winn et al. 2006) that can be significant in rapidly rotating stars F-stars. Bastien et al. (2014) have suggested that F-stars have been found to have more vigorous convective motions despite being magnetically inactive, and that the RV jitter is strongly correlated with the granulation flicker. We find that the offset between our  $\gamma_{RM}$  and  $\gamma$  values of  $\sim 100\text{m s}^{-1}$  is comparable to the RMS residual of the non-RM RV data. The results from the EXOFAST RM fit are shown in Figure 11.

For our final fits, we included all full and partial transits, all the radial velocities including the RM velocities, and we assumed a circular orbit with no RV slope. The stellar and planetary values derived using the YY stellar models and using the Torres relation are shown in Table 4 for comparison. We chose to adopt the YY model as our fiducial values. We find that the spin-orbit alignment determined from the global fit,  $\lambda = 9.7 \pm 5.2$  degrees, agrees with our independent solution discussed in Section 3.5. We also find that the resulting  $v \sin i$  from the global fit ( $v \sin i = 65_{-5}^{+6} \text{ km s}^{-1}$ ) is in close agreement with the results from SPC and our independent RM analysis.

The TTVs for all follow-up transits are shown in Figure 12. The global fit  $T_C$  and  $P$  were constrained only by the RV data and the priors imposed from the KELT discovery data. Using the follow-up transit light curves to constrain the ephemeris in the global fit would artificially reduce any observed TTV signal. As part of the global analysis, we fit as a free parameter a transit center time  $T_C$  for each transit shown in Table 3. A straight line was fit to all mid-transit times in Table 3, and shown in Figure 12, to derive a separate ephemeris from only the transit data. We find  $T_o = 2456355.229809 \pm 0.000198$ ,  $P = 2.7347785 \pm 0.0000038$ , with a  $\chi^2$  of 27.58 and 8 degrees of freedom. While the  $\chi^2$  is much larger than one might initially expect, this is likely due to systemat-

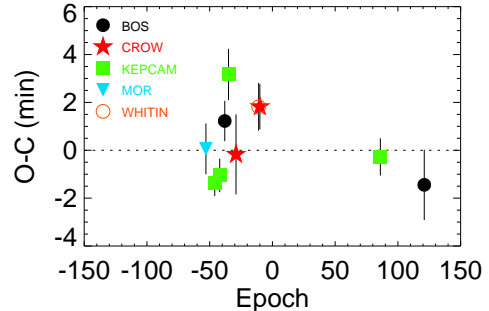


**Figure 12.** The residuals of the transit times from the best-fit ephemeris. The transit times are given in Table 3. The WHITIN observations at epoch -13 are hidden behind the CROW observations at epoch -12.

ics in the transit data from the ground-based photometry. Properly removing systematics in the partial transit data would be difficult, so we are therefore not convinced that this is evidence for TTVs. We were careful to check that all timestamps were in  $BJD_{TDB}$  time system using Eastman et al. (2010) to convert timestamps. Further studies would be required to rule out TTVs.

#### 4. FALSE POSITIVE ANALYSIS

There are many signals that could be mistaken for a planetary transit, so it is important to address some of these false positive scenarios. There are several reasons to favor a planetary signal over a false positive scenario for KELT-7b.

KELT has a very small aperture, and thus a very large point spread function (PSF), so many initial detections turn out to be blended starlight from more than one star in the PSF mimicking a transit signal. Therefore, it is important that we follow up our initial detection with seeing-limited telescopes (i.e., with PSFs of  $\sim 1''$ ) to rule out any blended eclipsing binaries. Observations using larger telescope in multiple filters then resolve stars that are blended even at the  $1''$  resolution, which typically turn out to be bound systems such as hierarchical triples. Our follow-up transits were observed in several different bandpasses (*Vgriz*), and we found no evidence of a wavelength-dependent transit depth.

We carefully inspected our spectra to look for light from another source. We did not see any evidence for the spectrum being double- or triple-lined. Our bisector analysis of the RVs taken out of transit showed no indication of being in phase with the orbital solution but we do see a correlation between bisector variation and RV variation of the spectra taken during transit due to the RM effect.

Our global fit with all spectroscopic and photometric data is well modeled by that of a transiting planet around a single star. We find that the  $\log g$  derived from our global fit,  $4.149 \pm 0.019$ , is consistent within errors to  $\log g$  derived from our SPC analysis,  $4.23 \pm 0.1$ . The amplitude of the RM signal is consistent with that expected from the  $v \sin i$  measured from the stellar spectrum and the depth and impact parameter measured from the high-precision transit light curves (see Section 3.5 and Section 3.7).

Finally, we obtained AO images, which exclude companion sources beyond a distance of  $0.1''$ ,  $0.2''$ ,  $0.5''$  and

**Table 4**  
Median values and 68% confidence interval for KELT-7b

Parameter	Units	YY-isocrone Values (adopted)	Torres Values
Stellar Parameters:			
$M_*$	Mass ( $M_\odot$ )	$1.535^{+0.066}_{-0.054}$	$1.483^{+0.069}_{-0.068}$
$R_*$	Radius ( $R_\odot$ )	$1.732^{+0.043}_{-0.045}$	$1.715 \pm 0.049$
$L_*$	Luminosity ( $L_\odot$ )	$5.73^{+0.37}_{-0.36}$	$5.61^{+0.39}_{-0.37}$
$\rho_*$	Density (cgs)	$0.419^{+0.027}_{-0.025}$	$0.415^{+0.029}_{-0.026}$
$\log g_*$	Surface gravity (cgs)	$4.149 \pm 0.019$	$4.140 \pm 0.019$
$T_{\text{eff}}$	Effective temperature (K)	$6789^{+50}_{-49}$	$6789 \pm 49$
[Fe/H]	Metallicity	$0.139^{+0.075}_{-0.081}$	$0.113^{+0.080}_{-0.083}$
$v \sin I_*^a$	Rotational velocity ( $km s^{-1}$ )	$65.0^{+6.0}_{-5.9}$	$65.4^{+5.9}_{-5.8}$
$\lambda$	Spin-orbit alignment (degrees)	$9.7 \pm 5.2$	$9.5^{+5.2}_{-5.1}$
Planetary Parameters:			
$P$	Period (days)	$2.7347749 \pm 0.0000039$	$2.7347750^{+0.0000040}_{-0.0000039}$
$a$	Semi-major axis (AU)	$0.04415^{+0.00062}_{-0.00052}$	$0.04364^{+0.00067}_{-0.00068}$
$M_P$	Mass ( $M_J$ )	$1.28 \pm 0.18$	$1.25 \pm 0.18$
$R_P$	Radius ( $R_J$ )	$1.533^{+0.046}_{-0.047}$	$1.514^{+0.051}_{-0.050}$
$\rho_P$	Density (cgs)	$0.442^{+0.073}_{-0.068}$	$0.446^{+0.074}_{-0.069}$
$\log g_P$	Surface gravity	$3.131^{+0.061}_{-0.068}$	$3.130^{+0.060}_{-0.068}$
$T_{eq}$	Equilibrium temperature (K)	$2048 \pm 27$	$2051^{+28}_{-27}$
$\Theta$	Safronov number	$0.0480^{+0.0069}_{-0.0067}$	$0.0486 \pm 0.0068$
$\langle F \rangle$	Incident flux ( $10^9 \text{ erg s}^{-1} \text{ cm}^{-2}$ )	$4.00^{+0.21}_{-0.20}$	$4.02^{+0.22}_{-0.21}$
RV Parameters:			
$T_C$	Time of inferior conjunction (BJD <sub>TDB</sub> )	$2456223.9592 \pm 0.0017$	$2456223.9591 \pm 0.0017$
$K_{RV}$	RV semi-amplitude ( $m s^{-1}$ )	$138 \pm 19$	$138 \pm 19$
$K_{RM}$	RM semi-amplitude ( $m s^{-1}$ )	$542^{+51}_{-50}$	$543^{+51}_{-49}$
$M_P \sin i$	Minimum mass ( $M_J$ )	$1.28 \pm 0.18$	$1.24 \pm 0.18$
$M_P/M_*$	Mass ratio	$0.00080 \pm 0.00011$	$0.00081 \pm 0.00011$
$u$	RM linear limb darkening	$0.5729^{+0.0032}_{-0.0034}$	$0.5724^{+0.0034}_{-0.0036}$
$\gamma$	$m s^{-1}$	$-133 \pm 15$	$-133 \pm 15$
$\gamma_{rm}$	$m s^{-1}$	$-35 \pm 19$	$-34 \pm 19$
$f(m_1, m_2)$	Mass function ( $M_J$ )	$0.00000080^{+0.00000038}_{-0.00000028}$	$0.00000080^{+0.00000037}_{-0.00000029}$
Primary Transit Parameters:			
$R_P/R_*$	Radius of the planet in stellar radii	$0.09097^{+0.00065}_{-0.00064}$	$0.09074^{+0.00067}_{-0.00066}$
$a/R_*$	Semi-major axis in stellar radii	$5.49^{+0.12}_{-0.11}$	$5.47 \pm 0.12$
$i$	Inclination (degrees)	$83.76^{+0.38}_{-0.37}$	$83.72^{+0.40}_{-0.39}$
$b$	Impact parameter	$0.597^{+0.022}_{-0.025}$	$0.599^{+0.023}_{-0.026}$
$\delta$	Transit depth	$0.00828 \pm 0.00012$	$0.00823 \pm 0.00012$
$T_0$	Best-fit linear ephemeris from transits (BJD <sub>TDB</sub> )	$2456355.229809 \pm 0.000198$	$2456352.495016 \pm 0.000191$
$P_{Ttransit}$	Best-fit linear ephemeris period from transits (days)	$2.7347785 \pm 0.0000038$	$2.7347795 \pm 0.0000037$
$T_{FWHM}$	FWHM duration (days)	$0.12795 \pm 0.00046$	$0.12821 \pm 0.00047$
$\tau$	Ingress/egress duration (days)	$0.01835^{+0.00092}_{-0.00089}$	$0.01840^{+0.00096}_{-0.00093}$
$T_{14}$	Total duration (days)	$0.14630^{+0.00097}_{-0.00092}$	$0.14662 \pm 0.00098$
$P_T$	A priori non-grazing transit probability	$0.1655 \pm 0.0034$	$0.1662^{+0.0035}_{-0.0036}$
$P_{T,G}$	A priori transit probability	$0.1987^{+0.0043}_{-0.0042}$	$0.1993^{+0.0044}_{-0.0045}$
Secondary Eclipse Parameters:			
$T_S$	Time of eclipse (BJD <sub>TDB</sub> )	$2456222.5918 \pm 0.0017$	$2456222.5918 \pm 0.0017$

<sup>a</sup> We adopted the SPC value for  $v \sin i$  ( $73 \text{ km s}^{-1}$ ) as our fiducial value since the EXOFAST RM analysis is not designed to model rapidly rotating stars.

1.0'' from KELT-7 down to a magnitude difference of 2.5 mag, 5.4 mag, 6.4 mag and 7.3 mag respectively, at a confidence level of  $5\sigma$  (see Figure 6).

We conclude that all the evidence is best described by a transiting hot Jupiter planet orbiting a rapidly rotating F-star. There is no significant evidence suggesting that the signal is better described from blended sources.

## 5. DISCUSSION

We have presented the discovery of KELT-7b, a hot Jupiter planet orbiting the ninth brightest star to host a known transiting planet. This is the fifth most massive star and fifth hottest star to host a transiting planet. Figure 13 shows the V magnitude versus transit depth for known transiting systems with  $V < 11$ , with the KELT discoveries highlighted. KELT-7b is an excellent candidate for future detailed atmospheric studies because it is a bright host star and it has a relatively deep transit. Although we suspect that it may be due to background



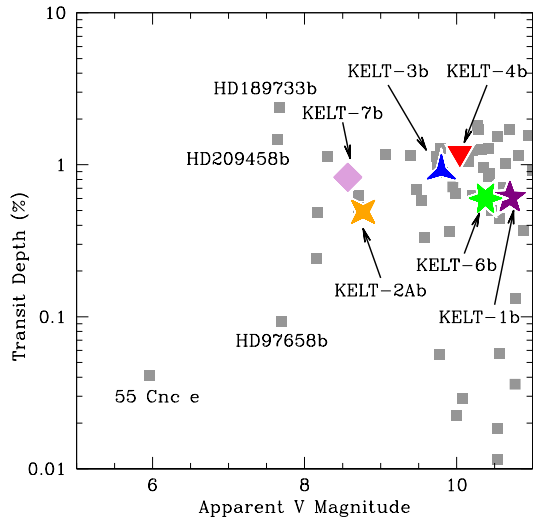


**Figure 13.** Transit depth as a function of apparent V magnitude of the host star for a sample of transiting systems with bright ( $V \leq 11$ ) hosts. KELT-7b is shown as a pink diamond. Bright stars with deep transits are generally the best targets for detailed follow-up.

nebulousity because the star lies in a region of considerably higher IR nebulousity than its surroundings, the slight IR excess we find at 22 microns can be confirmed or excluded using follow up observations.

KELT-7 is a rapidly rotating star with a  $v \sin i$  of  $73 \text{ km s}^{-1}$ . Measuring the reflex orbital motion is not easy for such a rapidly rotating star, and to date this is the most rapidly rotating transiting system to have this motion measured. The fast rotation also allowed us to measure the RM effect and measure the projected obliquity of the system. Understanding the projected spin-orbit alignment of a planet and host star can allow us to infer information about the formation and evolution of hot Jupiters. Winn et al. (2010) and Schlaufman (2010), by different methods, proposed that hot stars ( $T_{\text{eff}} > 6250 \text{ K}$ ) that host a transiting hot Jupiter typically have high stellar obliquity. Winn et al. (2010) suggested that hot Jupiter systems initially have a broad range of obliquities, but the cool stars eventually realign with the orbits of their companions because they undergo more rapid tidal dissipation than hot stars. Albrecht et al. (2012) did an RM analysis on a sample that nearly doubled the Winn et al. (2010) sample and confirmed the correlation of projected obliquity and the effective temperature of the star. Albrecht et al. (2012) also showed that the obliquity of systems with close-in massive planets have a dependence on the mass ratio and the distance between the star and planet. Specifically, they found that higher obliquities are measured in systems where the planet is relatively small.

The KELT-7 system consists of a transiting hot Jupiter on a fairly close orbit ( $a = 0.04 \text{ AU}$ ) to its massive and hot host star. We measured the system to have a low stellar obliquity ( $\lambda = 9.7 \pm 5.2$  degrees). One might expect that this planet formed with a low obliquity and migrated in close to the star because it has been suggested that if the planet formed around a hot host star with a high obliquity it would be unable to realign due to the lack of convective envelope. With a larger sample of hot

stars with transiting planets with projected obliquities, it will become possible to disentangle the dependences of stellar effective temperature, age, planet mass, and orbital distance on the projected obliquity. Ultimately, this will enable a deeper understanding of how systems form and evolve over time, and allow us to distinguish which systems are truly unique.

*Acknowledgements*— This paper uses observations obtained with facilities of the Las Cumbres Observatory Global Telescope. The Byrne Observatory at Sedgwick (BOS) is operated by the Las Cumbres Observatory Global Network and is located at the Sedgwick Reserve, as part of the University of California Natural Reserve System.

This material is based on work supported by the National Science Foundation Graduate Research Fellowship under Grant No. 2014184874. Any opinions, findings, and conclusions or recommendations expressed in this material are those of the authors and do not necessarily reflect the views of the National Science Foundation.

This work was performed in part under contract with the California Institute of Technology (Caltech)/Jet Propulsion Laboratory (JPL) funded by NASA through the Sagan Fellowship Program executed by the NASA Exoplanet Science Institute.

We would also like to thank Iain McDonald for his conversations about the data regarding the IR excess detected in the SED analysis.

## REFERENCES

- Alard, C., & Lupton, R. H. 1998, *ApJ*, 503, 325  
 Alard, C. 2000, *A&AS*, 144, 363  
 Albrecht, S., Winn, J. N., Johnson, J. A., et al. 2012, *ApJ*, 757, 18  
 Alonso, R., Brown, T. M., Torres, G., et al. 2004, *ApJ*, 613, L153  
 Bakos, G. Á., Noyes, R. W., Kovács, G., et al. 2007, *ApJ*, 656, 552  
 Bakos, G. Á., Csabry, Z., Penev, K., et al. 2013, *PASP*, 125, 154  
 Barnes, S. A. 2007, *ApJ*, 669, 1167  
 Bastien, F. A., Stassun, K. G., Pepper, J., et al. 2014, *AJ*, 147, 29  
 Batalha, N. M., Borucki, W. J., Koch, D. G., et al. 2010, *ApJ*, 713, L109  
 Beatty, T. G., Pepper, J., Siverd, R. J., et al. 2012, *ApJ*, 756, L39  
 Bensby, T., Feltzing, S., & Lundström, I. 2003, *A&A*, 410, 527  
 Bouchy, F., Bonomo, A. S., Santerne, A., et al. 2011, *A&A*, 533, A83  
 Bowler, B. P., Johnson, J. A., Marcy, G. W., et al. 2010, *ApJ*, 709, 396  
 Buchhave, L. A., Bakos, G. Á., Hartman, J. D., et al. 2010, *ApJ*, 720, 118  
 Buchhave, L. A., Latham, D. W., Johansen, A., et al. 2012, *Nature*, 486, 375  
 Carter, J. A., Winn, J. N., Holman, M. J., et al. 2011, *ApJ*, 730, 82  
 Chabrier, G., & Baraffe, I. 2000, *ARA&A*, 38, 337  
 Charbonneau, D., Brown, T. M., Latham, D. W., & Mayor, M. 2000, *ApJ*, 529, L45  
 Claret, A., & Bloemen, S. 2011, *A&A*, 529, A75  
 Collier Cameron, A., Wilson, D. M., West, R. G., et al. 2007, *MNRAS*, 380, 1230  
 Collier Cameron, A., Guenther, E., Smalley, B., et al. 2010, *MNRAS*, 407, 507  
 Collins, K. A., Eastman, J. D., Beatty, T. G., et al. 2014, *AJ*, 147, 39  
 Cutri, R. M., Skrutskie, M. F., van Dyk, S., et al. 2003, *VizieR Online Data Catalog*, 2246, 0  
 Cutri, R. M., & et al. 2012, *VizieR Online Data Catalog*, 2311, 0  
 Demarque, P., Woo, J.-H., Kim, Y.-C., & Yi, S. K. 2004, *ApJS*, 155, 667

- Eastman, J., Siverd, R., & Gaudi, B. S. 2010, *PASP*, 122, 935
- Eastman, J., Gaudi, B. S., & Agol, E. 2013, *PASP*, 125, 83
- Fulton, B. J., Shporer, A., Winn, J. N., et al. 2011, *AJ*, 142, 84
- Fűresz, G. 2008, PhD thesis, Univ. of Szeged, Hungary
- Gould, A., Pepper, J., & DePoy, D. L. 2003, *ApJ*, 594, 533
- Hartman, J. D., Gaudi, B. S., Holman, M. J., et al. 2008, *ApJ*, 675, 1233
- Hauschildt, P. H., Allard, F., Ferguson, J., Baron, E., & Alexander, D. R. 1999, *ApJ*, 525, 871
- Henry, G. W., Marcy, G. W., Butler, R. P., & Vogt, S. S. 2000, *ApJ*, 529, L41
- Hirano, T., Suto, Y., Winn, J. N., et al. 2011, *ApJ*, 742, 69
- Høg, E., Fabricius, C., Makarov, V. V., et al. 2000, *A&A*, 355, L27
- Howell, S. B., Sobek, C., Haas, M., et al. 2014, *PASP*, 126, 398
- Irwin, J., Charbonneau, D., Nutzman, P., & Falco, E. 2009, *IAU Symposium*, 253, 37
- Irwin, J. M., Berta-Thompson, Z. K., Charbonneau, D., et al. 2014, *arXiv:1409.0891*
- Jensen, E. 2013, *Astrophysics Source Code Library*, 6007
- Johnson, J. A., Morton, T. D., & Wright, J. T. 2013, *ApJ*, 763, 53
- Kovács, G., Zucker, S., & Mazeh, T. 2002, *A&A*, 391, 369
- Kovács, G., Bakos, G., & Noyes, R. W. 2005, *MNRAS*, 356, 557
- Kraft, R. P. 1970, *Spectroscopic Astrophysics. An Assessment of the Contributions of Otto Struve*, 385
- Kraft, R. P. 1967, *ApJ*, 150, 551
- Kurucz, R. L. 1992, *The Stellar Populations of Galaxies*, 149, 225
- Lloyd, J. P. 2013, *ApJ*, 774, LL2
- Martin, D. C., Fanson, J., Schiminovich, D., et al. 2005, *ApJ*, 619, L1
- McCullough, P. R., Stys, J. E., Valenti, J. A., et al. 2006, *ApJ*, 648, 1228
- McDonald, I., Zijlstra, A. A., & Boyer, M. L. 2012, *MNRAS*, 427, 343
- McLaughlin, D. B. 1924, *ApJ*, 60, 22
- Myers, J. R., Sande, C. B., Miller, A. C., Warren, W. H., Jr., & Tracewell, D. A. 2001, *VizieR Online Data Catalog*, 5109, 0
- Ohta, Y., Taruya, A., & Suto, Y. 2005, *ApJ*, 622, 1118
- Pepper, J., Pogge, R. W., DePoy, D. L., et al. 2007, *PASP*, 119, 923
- Pepper, J., Siverd, R. J., Beatty, T. G., et al. 2013, *ApJ*, 773, 64
- Perryman, M. A. C., Lindegren, L., Kovalevsky, J., et al. 1997, *A&A*, 323, L49
- Reiners, A., & Schmitt, J. H. M. M. 2003, *A&A*, 398, 647
- Ribas, Á., Merín, B., Ardila, D. R., & Bouy, H. 2012, *A&A*, 541, AA38
- Richmond, M. W., Droege, T. F., Gombert, G., et al. 2000, *PASP*, 112, 397
- Ricker, G. R., Winn, J. N., Vanderspek, R., et al. 2014, *Proc. SPIE*, 9143, 914320
- Rieke, G. H., Su, K. Y. L., Stansberry, J. A., et al. 2005, *ApJ*, 620, 1010
- Rossiter, R. A. 1924, *ApJ*, 60, 15
- Sanchis-Ojeda, R., Winn, J. N., Marcy, G. W., et al. 2013, *ApJ*, 775, 54
- Schlaufman, K. C. 2010, *ApJ*, 719, 602
- Siegler, N., Muzerolle, J., Young, E. T., et al. 2007, *ApJ*, 654, 580
- Siverd, R. J., Beatty, T. G., Pepper, J., et al. 2012, *ApJ*, 761, 123
- Stetson, P. B. 1987, *PASP*, 99, 191
- Skrutskie, M. F., Cutri, R. M., Stiening, R., et al. 2006, *AJ*, 131, 1163
- Torres, G., Andersen, J., & Giménez, A. 2010, *A&A Rev.*, 18, 67
- Trilling, D. E., Bryden, G., Beichman, C. A., et al. 2008, *ApJ*, 674, 1086
- van Saders, J. L., & Pinsonneault, M. H. 2012, *ApJ*, 746, 16
- van Saders, J. L., & Pinsonneault, M. H. 2013, *ApJ*, 776, 67
- Winn, J. N., Johnson, J. A., Marcy, G. W., et al. 2006, *ApJ*, 653, L69
- Winn, J. N., Fabrycky, D., Albrecht, S., & Johnson, J. A. 2010, *ApJ*, 718, L145
- Wizinowich, P. L. 2000, *Proc. SPIE*, 4007,
- Wright, J. T., Marcy, G. W., Butler, R. P., & Vogt, S. S. 2004, *ApJS*, 152, 261
- Wright, E. L., Eisenhardt, P. R. M., Mainzer, A. K., et al. 2010, *AJ*, 140, 1868
- Wyatt, M. C. 2008, *ARA&A*, 46, 339
- Zacharias, N., Monet, D. G., Levine, S. E., et al. 2004, *Bulletin of the American Astronomical Society*, 36, 1418
- Zacharias, N., Finch, C. T., Girard, T. M., et al. 2013, *AJ*, 145, 44